Hindawi Publishing Corporation
Advances in OptoElectronics
Volume 2012, Article ID 736876, 9 pages
doi:10.1155/2012/736876

Research Article

Realization of Radar Illusion Using Active Devices

B. Z. Cao,[1,2] L. Sun,[1] and Z. L. Mei[1,2]

[1] *School of Information Science and Engineering, Lanzhou University, Lanzhou 730000, China*
[2] *State Key Laboratory of Millimeter Waves, Southeast University, Nanjing 210096, China*

Correspondence should be addressed to Z. L. Mei, meizl@lzu.edu.cn

Received 2 July 2012; Revised 10 September 2012; Accepted 19 September 2012

Academic Editor: Alexandra E. Boltasseva

A new method is proposed for realizing radar illusion of an electromagnetic target by using active devices. The devices are installed around the target but may closely cover the target or not, leading to closed or open configurations. The amplitudes and phases of the active devices are determined by using T-matrix method. The numerical computation is calculated using MATLAB, and the results show that this method is convenient, flexible, and efficient, which has important significances for implementation of novel electromagnetic devices.

1. Introduction

Since invisible cloaking using metamaterials was theoretically proposed and experimentally demonstrated in 2006 [1, 2], various methods have been put forward for realizing this fabulous electromagnetic (EM) phenomenon [1–8]. Generally speaking, EM invisibility, or illusion in general, can be roughly divided into four categories: (1) rendering the object transparent or invisible by controlling the parameters of metamaterials based on the scattering cancellation theory [7, 9]; (2) making the object invisible or illusory by exploiting the abnormal EM properties and the special ability to control EM waves of metamaterials based on the transformation optics theory [10, 11]; (3) invisibility using anomalous localized resonance method [12, 13]; (4) realizing invisibility or illusion using the surface integral equation of the EM field based on active devices [14–18]. So far, realization of radar illusion for an EM target is mainly based on the method of transformation optics [19–26]. Compared with the transformation optics method, active devices can be designed to work at a broadband of frequencies and do not need materials with extreme parameters. However, only a few works on radar illusion have been reported for an object by using active devices [17, 18], to the best of our knowledge.

In this paper, we use two kinds of active devices to realize the radar illusion of an object. One is called the closed configuration, where the active devices are set around and closely wrap the object. The other is called open configuration, where the active devices are deployed around the object but do not cover it. The drawback of the former one is that signals from outside have been blocked, leading to poor communication for the target, while the latter does not affect the information transmission. Compared to the previous works [14–18], our scheme can not only make an object invisible to the outsider but also mimic a totally different object at a different place. It is thus a direct extension of the original work. In the next section, the two kinds of active devices are designed and simulated, and errors are analyzed. Though only rotation and virtual shift effects are studied in the paper, other illusion effects can be realized using the same method, including superscattering, geometry change, and parameter transformation [22–25]. Hence the method has important applications in military sectors. We remark that the method has its weakness, and a serious drawback is that the probing wave must be known in advance [14–16].

2. Theory Analysis

For simplicity, we only consider problems in the two-dimensional (2D) situation. The schematic diagrams of active devices to realize virtual rotation and shift are shown in Figure 1. In Figure 1(a), the real object (a green-colored hexagon) is put at the bottom side, and it will appear at

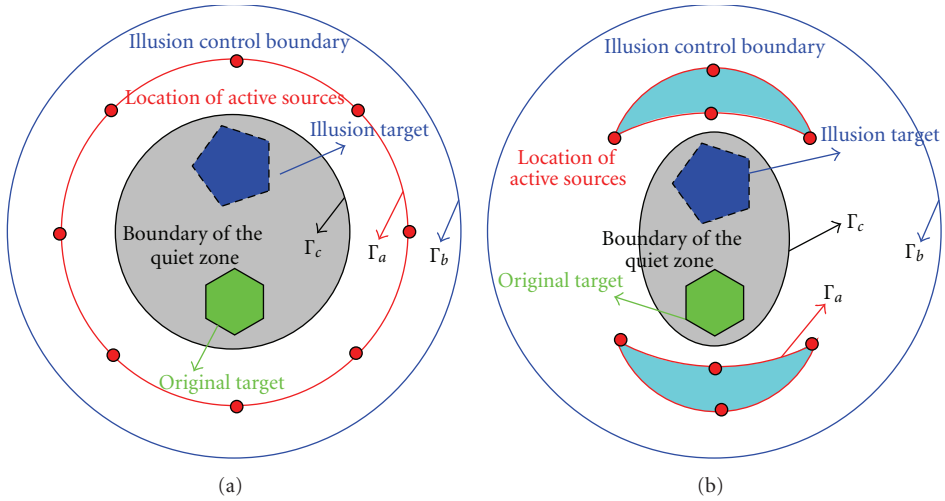

Figure 1: Schematic diagrams of the proposed active device to realize radar illusion. (a) Closed configuration; (b) open configuration.

the top side by using closed devices which are set along its periphery (Γ_a in the figure). The position of the active device, the boundary of the controlling illusion, and that of the quiet zone are expressed as Γ_a, Γ_b, and Γ_c, respectively. Figure 1(b) depicts the radar illusion using an open configuration. In this case, the active device is deployed near the device but does not cover it, which is important for practical applications. The shift of the object can also be realized by using the active devices which are deployed on the boundary Γ_a. In both cases, an outsider will see a virtually shifted pentagon instead of the hexagon, that is, radar illusion.

Suppose the probing wave works at ω, then the wave function $u(\mathbf{r}, t)$ satisfies Helmholtz's equation

$$\nabla^2 u + k^2 u = 0, \tag{1}$$

where $k = 2\pi/\lambda$ is the wave number, $\lambda = 2\pi c/\omega$ is the wavelength, and c is the velocity of light.

For an arbitrary incident wave u_{inc}, the cancellation field generated by the active devices on Γ_c is required to assure a zero total field in the "quiet zone," as its name suggests. So any object in this region has no scattering at all. At the same time, the active devices will generate a properly designed scattering field on Γ_b so that an external observer will see a different object at a different location and probably with different EM "fingerprint," that is, radar illusion. When that specific field is set to zero, it means the object is totally shielded from the outsider. However, if the scattered field on Γ_b is consistent with what is generated by another object at another place without active devices, it means the virtual shifting effect is realized. Other illusions can be implemented using the same methodology.

Since the active devices can be considered as a series of line sources with certain distribution, the total fields radiated can be expressed by using the Fourier-Bessel series:

$$u_d(\boldsymbol{\rho}) = \sum_{m=1}^{M} \sum_{n=-N}^{N} a_{mn} H_n^{(1)}\left(k\left|\boldsymbol{\rho} - \boldsymbol{\rho}_m\right|\right) e^{jn\theta_m}, \tag{2}$$

where $H_n^{(1)}(x)$ is Hankel function of the first kind with order n, $\boldsymbol{\rho}$ represents an arbitrary position vector, $\boldsymbol{\rho}_m$ represents the position vector on Γ_a, and the angle $\theta_m = \arg(\boldsymbol{\rho} - \boldsymbol{\rho}_m)$ shows direction angle between the vector $\boldsymbol{\rho} - \boldsymbol{\rho}_m$ and the horizontal direction.

To realize virtual shift of an object, the boundary condition should be set to

$$u_d(\boldsymbol{\rho}) = \begin{cases} -u_{\text{inc}}(\boldsymbol{\rho}) & \forall \boldsymbol{\rho} \in \Gamma_c, \\ u_{\text{shift}}(\boldsymbol{\rho}) & \forall \boldsymbol{\rho} \in \Gamma_b, \end{cases} \tag{3}$$

where $u_{\text{shift}}(\boldsymbol{\rho})$ denotes the scattered field produced by a shifted object on Γ_b.

During numerical calculation, one must divide the boundaries into discrete points. In our design, we set number of points to M on Γ_a, M_b on Γ_b, and M_c on Γ_c, respectively. According to (3), the field on Γ_b and Γ_c can be expressed as

$$u_d\left(\boldsymbol{\rho}_i^b\right) = \sum_{m=1}^{M} \sum_{n=-N}^{N} a_{mn} H_n^{(1)}\left(k\left|\boldsymbol{\rho}_i^b - \boldsymbol{\rho}_m\right|\right) e^{jn\theta_m} \quad \forall \boldsymbol{\rho}_i^b \in \Gamma_b,$$

$$u_d\left(\boldsymbol{\rho}_j^c\right) = \sum_{m=1}^{M} \sum_{n=-N}^{N} a_{mn} H_n^{(1)}\left(k\left|\boldsymbol{\rho}_j^c - \boldsymbol{\rho}_m\right|\right) e^{jn\theta_m} \quad \forall \boldsymbol{\rho}_j^c \in \Gamma_c. \tag{4}$$

The coefficients a_{mn} can be found numerically by enforcing (3) on points $\boldsymbol{\rho}_1^b, \boldsymbol{\rho}_2^b, \ldots, \boldsymbol{\rho}_{M_b}^b$, and $\boldsymbol{\rho}_1^c, \boldsymbol{\rho}_2^c, \ldots, \boldsymbol{\rho}_{M_c}^c$ for boundary Γ_b and Γ_c, respectively. From (2), (3), and (4), the following linear equations can be obtained:

$$\begin{bmatrix} \mathbf{H}_b \\ \mathbf{H}_c \end{bmatrix} \begin{bmatrix} \mathbf{B} \\ \mathbf{C} \end{bmatrix} = \begin{bmatrix} \mathbf{U}_{\text{shift}} \\ -\mathbf{U}_{\text{inc}} \end{bmatrix}, \tag{5}$$

where $\mathbf{B} = [a_{1n}, a_{2n}, \ldots, a_{M_b n}]$, $\mathbf{C} = [a_{1n}, a_{2n}, \ldots, a_{M_c n}]$, $[\mathbf{H}_b] = H_n^{(1)}(k|\boldsymbol{\rho}^b - \boldsymbol{\rho}_m|)e^{jn\theta_m}$, $n \in [-N, N]$, and $[\mathbf{H}_c] = H_n^{(1)}(k|\boldsymbol{\rho}^c - \boldsymbol{\rho}_m|)e^{jn\theta_m}$. The equation $M(2N+1) = M_b + M_c$ must be maintained to ensure $\mathbf{H}$ as a square matrix.

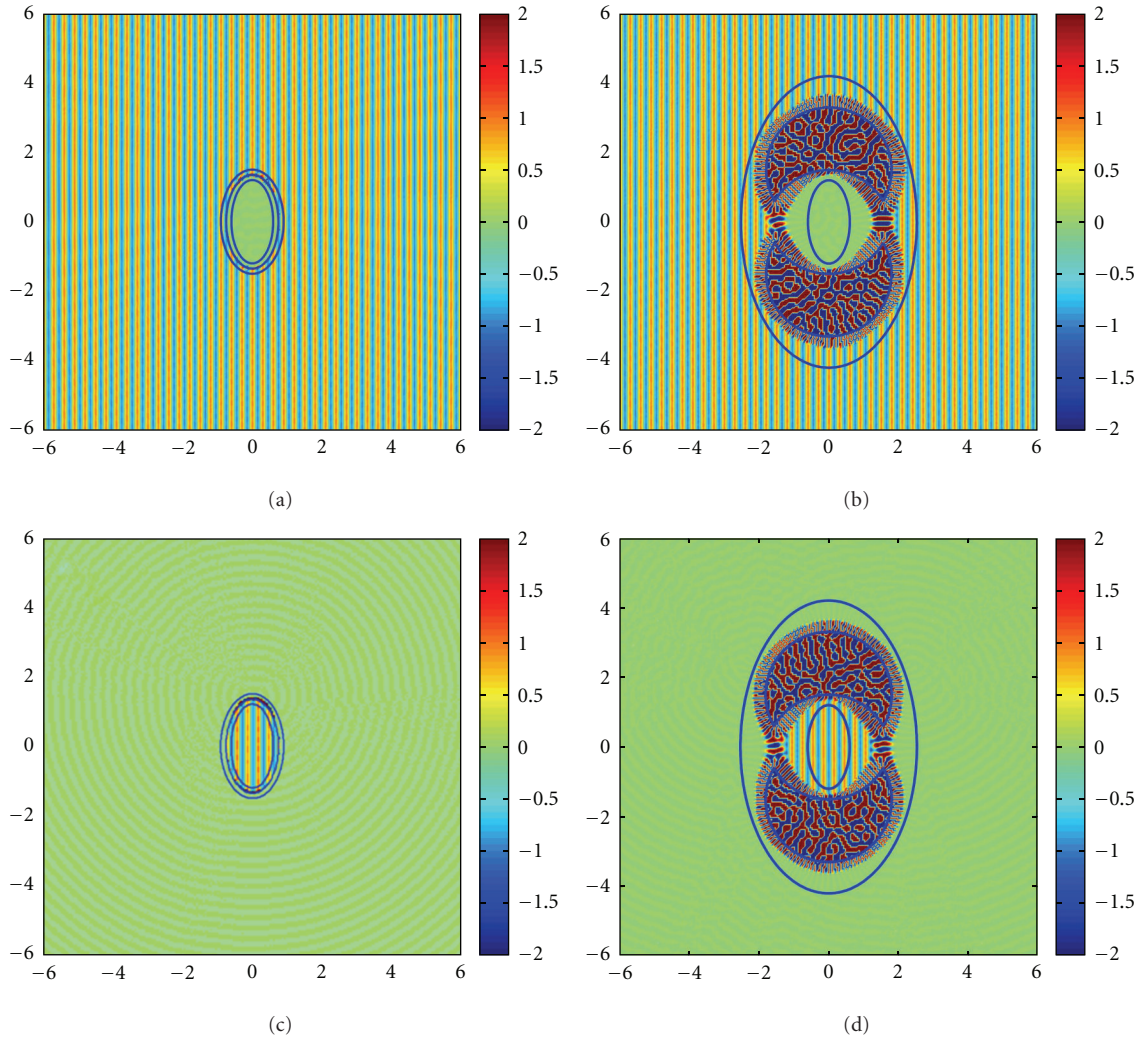

FIGURE 2: Numerical results for the active cloaking device. (a)-(b) Total fields for the closed and open configuration; (c)-(d) scattered fields for the closed and open configuration.

3. Numerical Calculation and Simulation for a Special Case

We first give the numerical calculation for a very special case, that is, invisibility cloaking using active devices. In this case, it is very clear that external and internal cloaking can be achieved by setting $u_{\text{shift}} = 0$ in (3). In the simulation, a rightward propagating plane wave $u_{\text{inc}} = e^{-jk_0x}$ is used as a probing wave just for its simplicity, but other forms of incident waves are applicable too. The total fields and the scattered fields for the two kinds of cloaking devices are shown in Figure 2, where Figures 2(a) and 2(b) show the total fields and Figures 2(c) and 2(d) show the scattered fields. In the left panels, where the closed configuration is demonstrated, active devices are uniformly placed on an elliptical curve, whose major axis is 1.35 m and the minor axis is 0.75 m. For the controlling boundary Γ_b, we set the major axis as 1.5 m and the minor axis as 0.9 m. While for Γ_c, the major axis is 1.2 m and the minor axis is 0.6 m. In the right panels, we show the open configuration in which the active devices are placed on two separated crescents. The major and minor axes for the controlling boundary Γ_b are 4.2 m and 2.52 m, respectively and those for Γ_c are 1.2 m and 0.6 m, respectively. In both cases, the following parameters are chosen, wavelength λ =0.3 m, $M(2N+1) = 630$, $M_c = 300$, and $M_b = 330$. Employing the scheme described in the preceding section, we can achieve an approximate solution numerically. We can see from Figure 2 that the field inside the quiet zone is essentially zero with no scattering.

In order to quantify the overall quality of the solution, we consider the following error functions on the boundary Γ_b and Γ_c:

$$\text{Err}(\Gamma_b) = \sum_{m=1}^{M_b} \frac{|u_d(\boldsymbol{\rho}) - u_{\text{shift}}(\boldsymbol{\rho})|}{|u_{\text{shift}}(\boldsymbol{\rho})|}, \quad \boldsymbol{\rho} \in \Gamma_b,$$
$$\text{Err}(\Gamma_c) = \sum_{m=1}^{M_c} \frac{|u_d(\boldsymbol{\rho}) + u_i(\boldsymbol{\rho})|}{|u_i(\boldsymbol{\rho})|}, \quad \boldsymbol{\rho} \in \Gamma_c. \tag{6}$$

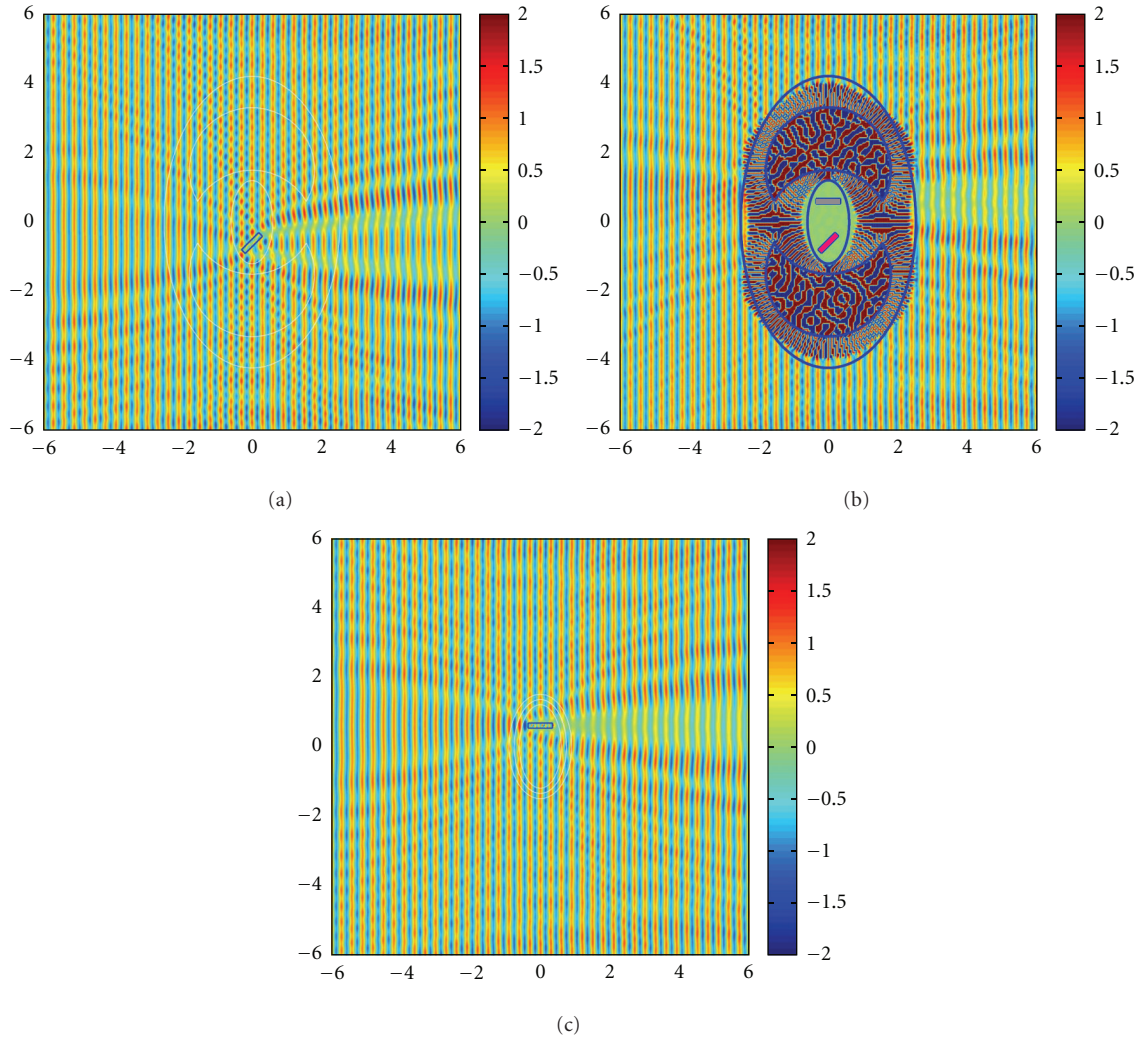

Figure 3: The virtual shift of a rectangular column using the open configuration. (a) Total fields distribution when the column is placed at (0, −0.6 m) with 45 degree to the horizon; (b) similar to (a) but the active device is turned on. (c) Total fields distribution when the column is placed at (0, 0.6 m) with zero degree to the horizon.

Table 1: The relationship between the errors on the boundary Γ_b, Γ_c and the values of N, M_b, and M_c for the cloak shown in Figure 2(a) ($M = 60$).

N	1	2	3	4	5	6	7	8	9	10	11	12
M_b	120	200	250	320	400	450	500	550	600	700	760	820
M_c	60	100	170	220	260	330	400	470	540	560	620	680
$\mathrm{Err}(\Gamma_c)$	2.5728 $e-005$	9.3572 $e-006$	1.3964 $e-005$	1.0182 $e-007$	4.6384 $e-007$	1.7500 $e-009$	1.1827 $e-008$	2.4238 $e-009$	8.3650 $e-012$	2.8560 $e-013$	1.5247 $e-012$	3.0913 $e-013$
$\mathrm{Err}(\Gamma_b)$	3.1699 $e-005$	1.1729 $e-005$	1.7795 $e-005$	1.2499 $e-007$	6.4917 $e-007$	2.4167 $e-009$	2.6140 $e-008$	4.7026 $e-009$	9.8610 $e-012$	3.7850 $e-013$	2.1948 $e-012$	4.0417 $e-013$

The calculated errors on Γ_b and Γ_c are given in Tables 1 and 2 for the two configurations mentioned above, where Table 1 shows the errors for the internal cloak in Figure 2(a), and Table 2 shows the errors for the external cloak shown in Figure 2(b). From these two tables, it can be seen that the error decreases as we increase N. In other words, we are able to achieve better cloaking effects if we can control the boundary fields more precisely. At the same time, it can be seen that the errors depend on the choice of M, M_b, and M_c for a given working frequency, and the accuracy of the calculation is quite high. The results show that this method is convenient and flexible.

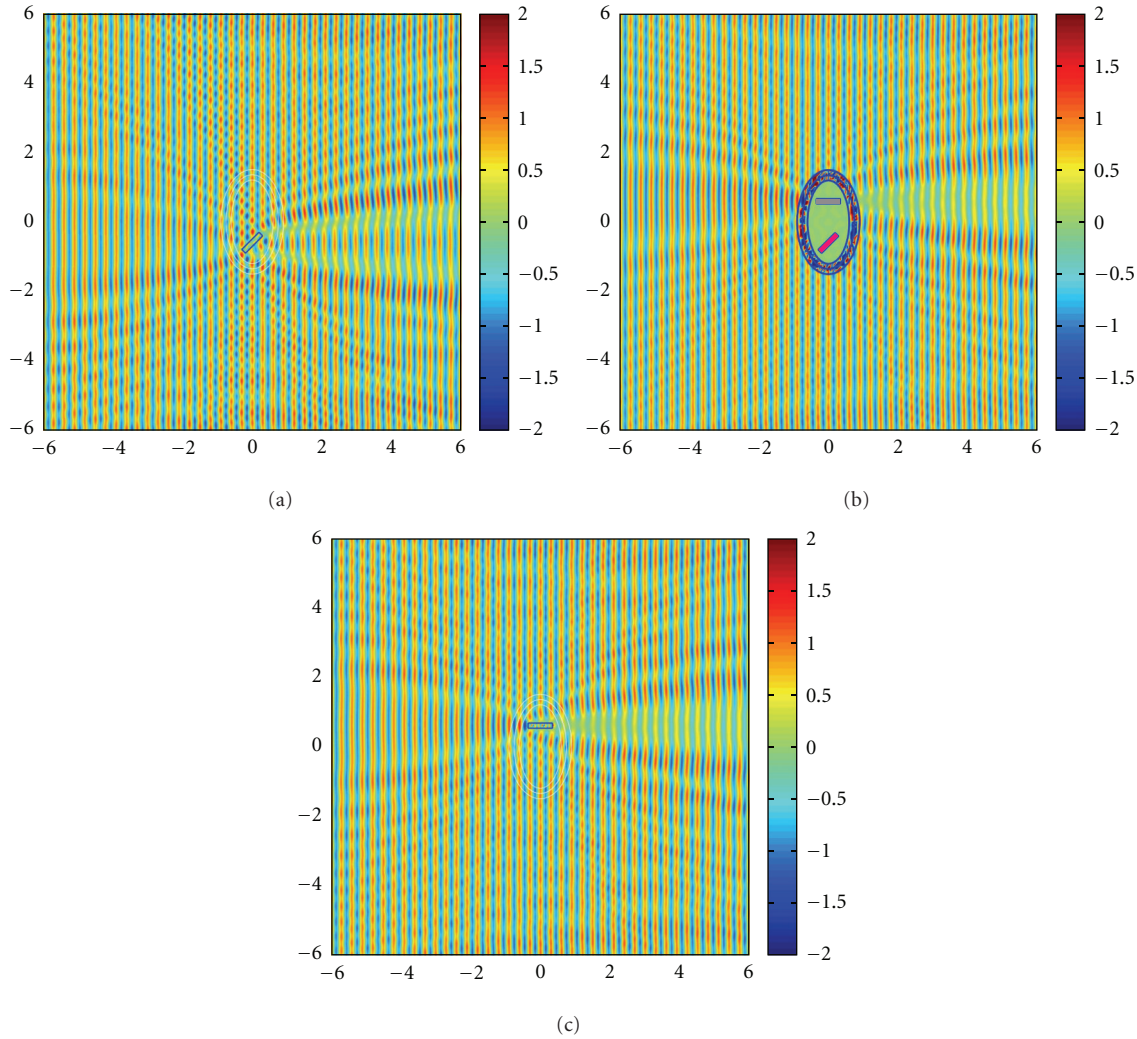

Figure 4: The virtual shift of a rectangular column using the closed configuration. (a) Total fields distribution when the column is placed at (0, −0.6 m) with 45 degree to the horizon; (b) similar to (a) but the active device is turned on. (c) Total fields distribution when the column is placed at (0, 0.6 m) with zero degree to the horizon.

Table 2: The relationship between the errors on the boundary Γ_b, Γ_c and the values of N, M_b, and M_c for the cloak shown in Figure 2(b) ($M = 60$).

N	1	2	3	4	5	6	7	8	9	10	11	12
M_b	120	200	250	320	400	450	500	550	600	700	760	820
M_c	60	100	170	220	260	330	400	470	540	560	620	680
$\mathrm{Err}(\Gamma_c)$	1.2086	9.7481 $e-005$	2.5488 $e-008$	2.8345 $e-008$	2.4315 $e-008$	1.8331 $e-008$	6.6296 $e-009$	1.8940 $e-009$	4.9820 $e-010$	8.9760 $e-011$	1.3725 $e-011$	4.6240 $e-012$
$\mathrm{Err}(\Gamma_b)$	1.4135	7.8877 $e-005$	2.3319 $e-008$	2.6458 $e-008$	2.5146 $e-008$	1.9514 $e-008$	8.9207 $e-009$	2.4907 $e-009$	7.2545 $e-010$	1.3302 $e-010$	1.9367 $e-011$	5.5004 $e-012$

4. Numerical Calculation and Simulation for Illusion of an Object

Next, we demonstrate the illusion effect where an object placed somewhere inside the quiet zone will appear at a different place. As an example, we choose a rectangular column with a cross-section of about $0.7 * 0.15\,\mathrm{m}^2$ and $\varepsilon_r = 10$, $\mu_r = 1$. The wavelength of the incoming plane wave is $\lambda = 0.3\,\mathrm{m}$. And other parameters are $M(2N + 1) = 630$, $M_c = 300$, and $M_b = 330$, respectively. Figure 3(a) shows the total fields when the rectangular column is located at (0, −0.6 m) with 45 degree to the horizon under the plane wave illumination, while Figure 3(c) gives similar results but the rectangular column is located at (0, 0.6 m)

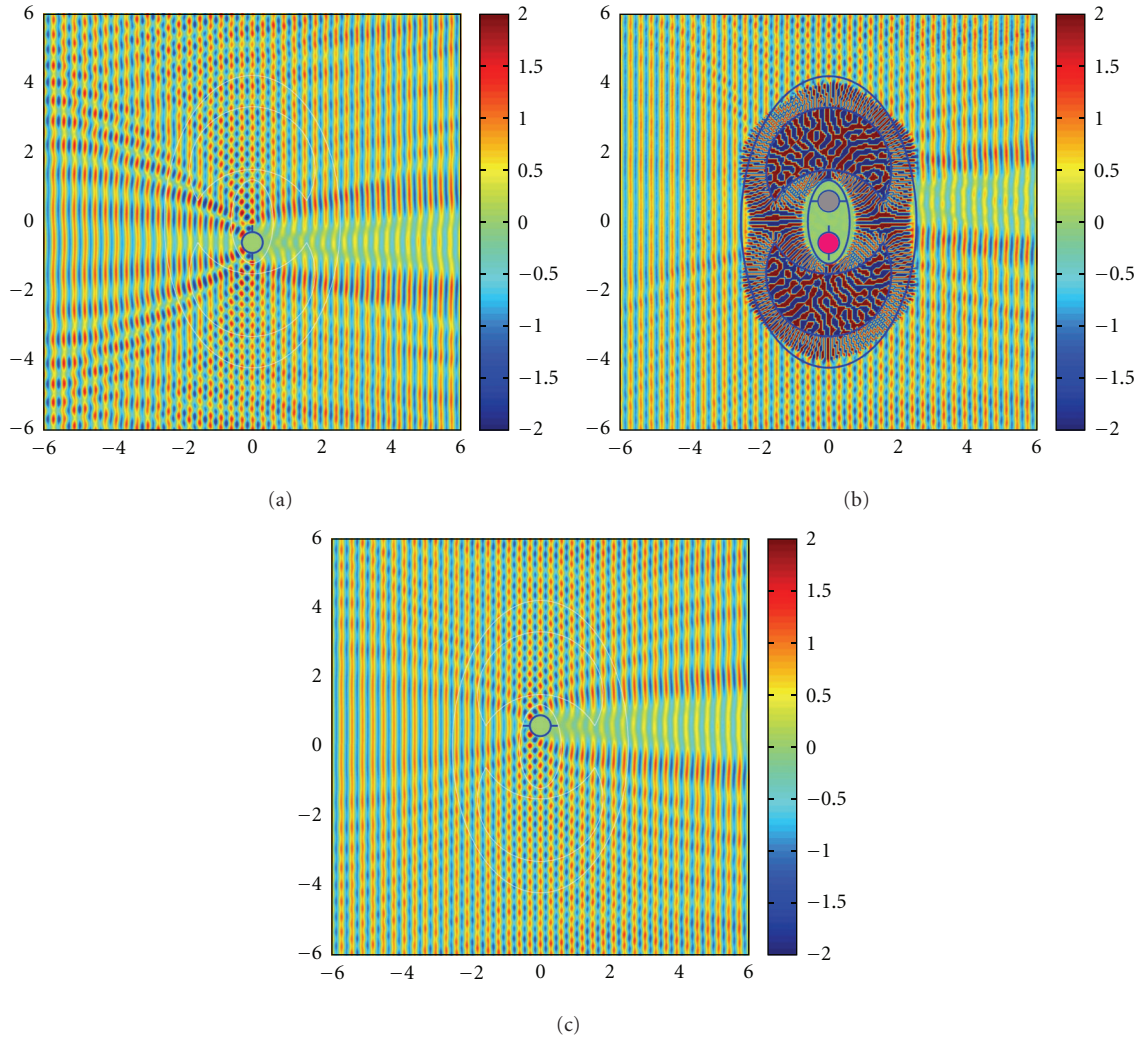

Figure 5: The virtual shift of a copper cylinder with a pair of metallic wings using the open configuration. (a) Total fields distribution when the column is placed at (0, −0.6 m) with 90 degree to the horizon; (b) similar to (a) but the active device is turned on. (c) Total fields distribution when the column is placed at (0, 0.6 m) with zero degree to the horizon.

with zero degree to the horizon; that is, it parallels to the horizontal line. In Figure 3(b), we show the total field of this rectangular column when the proposed active device shown in Figure 1(b) is turned on. Comparing Figure 3(b) with Figure 3(c) for the total fields outside the controlling boundary, we can see that they are very similar with each other. Therefore, the shift of the object is clearly realized together with a rotation. Figure 4 demonstrates similar results; however the closed configuration in Figure 1(a) is adopted.

Figures 5 and 6 show the virtual shift of a copper cylinder with a pair of metallic wings. The radius of the metal cylinder is about one wavelength. Other parameters are the same as those mentioned above. Figure 5(a) shows the total fields of this metal cylinder located at (0, −0.6 m) with the wings vertical to the horizon under the illumination of the plane wave. Figure 5(c) shows the total fields of the metal cylinder which is located at (0, 0.6 m) with the wings parallel to the horizon. And Figure 5(b) shows the total fields of this metal cylinder with the active devices shown in Figure 1(b) switched on. Careful comparison between Figure 5(b) with Figure 5(c) shows that the distribution of the EM wave is exactly the same for the two figures out of the controlling boundary, which is another proof of the shift and rotation effect using this method. Figure 6 shows the similar results using active devices depicted in Figure 1(a).

To quantitatively validate the performance of the active illusion device, we also calculate the normalized scattering width for different cases, and the results are shown in Figure 7. The detailed calculation process can be found in [26]. In Figure 7(a), we give the scattering width for the open configuration, whose near fields are demonstrated in Figure 5. A careful examination shows that the normalized scattering pattern for the vertically placed metallic cylinder, represented by the blue dotted line, differs greatly from the horizontally placed one at a different position (green sold line). However, when active sources are deployed around the former one, we obtain a very similar scattering pattern,

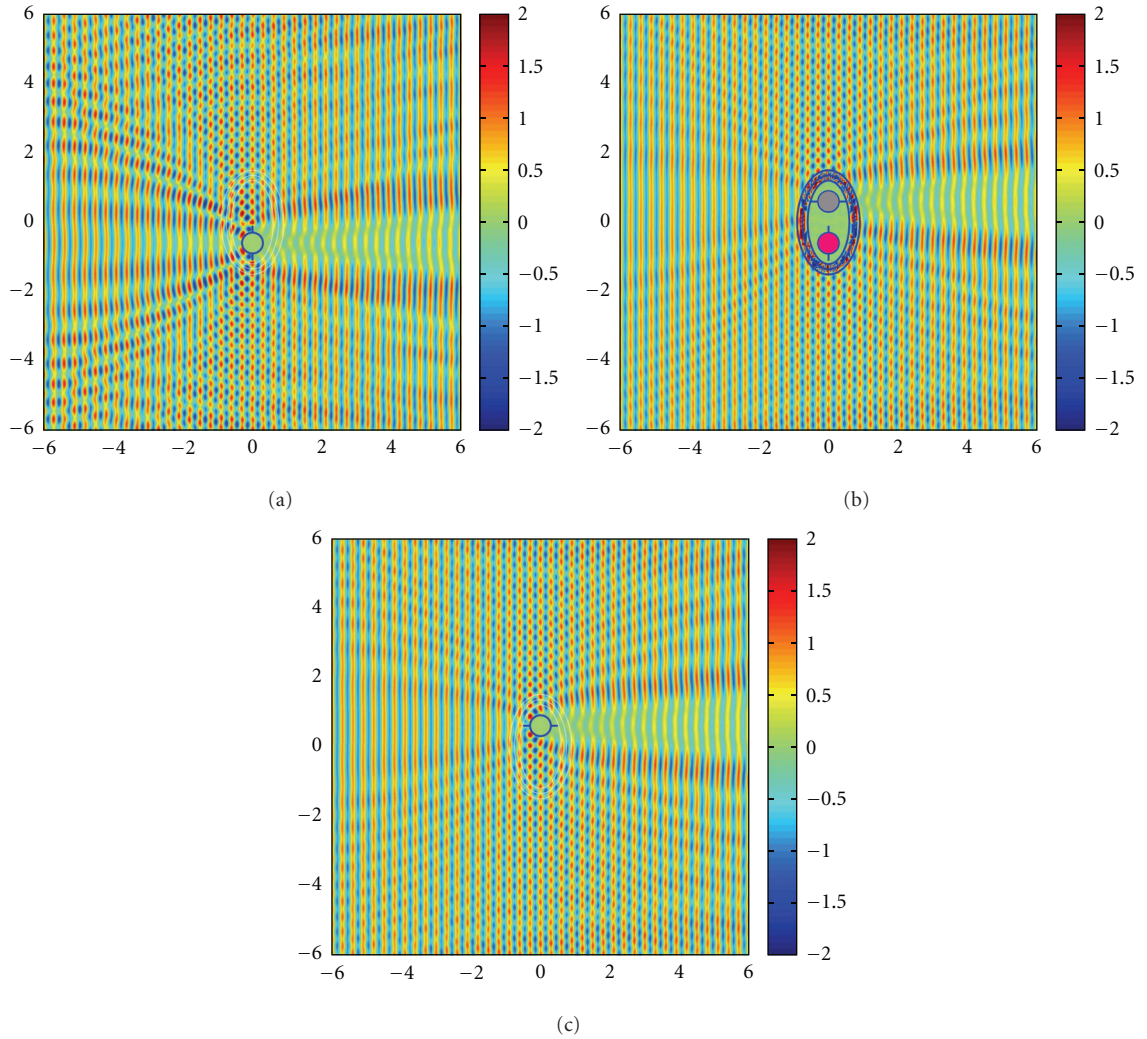

Figure 6: The virtual shift of a copper cylinder with a pair of metallic wings using the closed configuration. (a) Total fields distribution when the column is placed at (0, −0.6 m) with 90 degree to the horizon; (b) similar to (a) but the active device is turned on. (c) Total fields distribution when the column is placed at (0, 0.6 m) with zero degree to the horizon.

denoted by the red dash-dotted line. The differences mainly come from the following approximations: (1) limited terms used for Hankel's function, $N = 3$ in our case; (2) limited points on the control boundary, that is, Γ_b and Γ_c, which are 330 and 300 in our calculation; (3) limited sources on Γ_a, which we set to 90. As mentioned in the previous section, larger numbers can lead to better performances. Figure 7(b) shows similar result for the closed structure, whose field distributions are demonstrated in Figure 6. In this case, better performances are obtained using the same parameter. This observation may be explained by a more uniform source distribution around the vertically placed metallic cylinder, which is clearly shown in Figure 1.

5. Summary

This paper presents a new method for realizing radar illusion for an arbitrary object by using active devices. The numerical calculation and simulation in the 2D case are studied, which include both closed and open configurations, and the results firmly support our design. The method is convenient, flexible, efficient, and accurate. The work can be extended to three dimensions and to include other illusion effects [22–25]. The limitation of this type of radar illusion is that it requires the prior knowledge of the probing wave. However, with the development of modern digital signal processing technology, the result in this paper may have practical significance for realizing novel EM devices.

Acknowledgments

The authors are grateful for the financial support from the State Key Laboratory of Millimeter Waves under Grant no. K201115, Natural Science Foundation of Gansu Province (no. 1107RJZA181), the Chunhui Project (no. Z2010081),

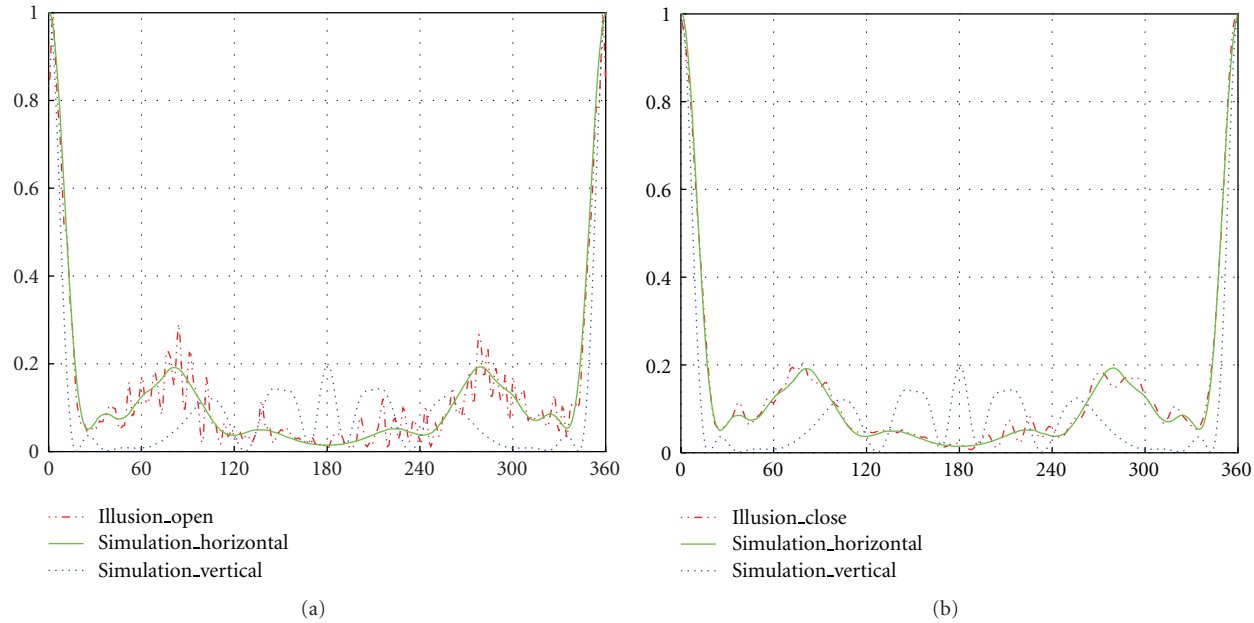

Figure 7: Normalized scattering width for different configurations. In the figure, x-axis represents the scanning angle (degree), and y-axis denotes the normalized scattering width. (a) The open configuration shown in Figure 5; (b) the closed configuration given in Figure 6.

and the Fundamental Research Funds for the Central Universities (no. LZUJBKY-2012-49).

References

[1] J. B. Pendry, D. Schurig, and D. R. Smith, "Controlling electromagnetic fields," *Science*, vol. 312, no. 5781, pp. 1780–1782, 2006.

[2] D. Schurig, J. J. Mock, B. J. Justice et al., "Metamaterial electromagnetic cloak at microwave frequencies," *Science*, vol. 314, no. 5801, pp. 977–980, 2006.

[3] B. Zhang, Y. Luo, X. Liu, and G. Barbastathis, "Macroscopic invisibility cloak for visible light," *Physical Review Letters*, vol. 106, no. 3, Article ID 033901, 2011.

[4] X. Chen, Y. Luo, J. Zhang, K. Jiang, J. B. Pendry, and S. Zhang, "Macroscopic invisibility cloaking of visible light," *Nature Communications*, vol. 2, article 176, 2011.

[5] G. W. Milton, M. Briane, and J. R. Willis, "On cloaking for elasticity and physical equations with a transformation invariant form," *New Journal of Physics*, vol. 8, no. 10, p. 248, 2006.

[6] H. F. Ma and T. J. Cui, "Three-dimensional broadband ground-plane cloak made of metamaterials," *Nature Communications*, vol. 1, article 21, 2010.

[7] A. Alu and N. Engheta, "Achieving transparency with plasmonic and metamaterial coatings," *Physical Review E*, vol. 72, no. 1, pp. 1–9, 2005.

[8] H. Chen, C. T. Chan, and P. Sheng, "Transformation opticsand metamaterials," *Nature Materials*, vol. 9, no. 5, pp. 387–396, 2010.

[9] L. Sun and K. W. Yu, "Broadband electromagnetic transparency by graded metamaterials: scattering cancellation scheme," *Journal of the Optical Society of America B*, vol. 28, no. 5, pp. 994–1001, 2011.

[10] W. Yan, M. Yan, Z. Ruan, and M. Qiu, "Coordinate transformations make perfect invisibility cloaks with arbitrary shape," *New Journal of Physics*, vol. 10, no. 4, pp. 1–13, 2008.

[11] Y. You, G. W. Kattawar, P. W. Zhai, and P. Yang, "Invisibility cloaks for irregular particles using coordinate transformations," *Optics Express*, vol. 16, no. 9, pp. 6134–6145, 2008.

[12] G. W. Milton and N. A. P. Nicorovici, "On the cloaking effects associated with anomalous localized resonance," *Proceedings of the Royal Society A*, vol. 462, no. 2074, pp. 3027–3059, 2006.

[13] N. A. P. Nicorovici, G. W. Milton, R. C. McPhedran, and L. C. Botten, "Quasistatic cloaking of two-dimensional polarizable discrete systems by anomalous resonance," *Optics Express*, vol. 15, no. 10, pp. 6314–6323, 2007.

[14] D. A. B. Miller, "On perfect cloaking," *Optics Express*, vol. 14, no. 25, pp. 12457–12466, 2006.

[15] F. G. Vasquez, G. W. Milton, and D. Onofrei, "Broadband exterior cloaking," *Optics Express*, vol. 17, no. 17, pp. 14800–14805, 2009.

[16] F. G. Vasquez, G. W. Milton, and D. Onofrei, "Active exterior cloaking for the 2D Laplace and Helmholtz equations," *Physical Review Letters*, vol. 103, no. 7, Article ID 073901, 2009.

[17] H. H. Zheng, J. J. Xiao, Y. Lai, and C. T. Chan, "Exterior optical cloaking and illusions by using active sources: a boundary element perspective," *Physical Review B*, vol. 81, no. 19, pp. 1–10, 2010.

[18] B. Z. Cao and L. Sun, "A new method for realizing illusion and shift of electromagnetic target based on active devices," in *Proceedings of the International Conference of Microwave and Millimeter Wave Technology (ICMMT '12)*, vol. 3, pp. 1–4, 2012.

[19] Y. Lai, J. Ng, H. Chen et al., "Illusion optics: the optical transformation of an object into another object," *Physical Review Letters*, vol. 102, no. 25, pp. 1–4, 2009.

[20] W. X. Jiang and T. J. Cui, "Moving targets virtually via composite optical transformation," *Optics Express*, vol. 18, no. 5, pp. 5161–5167, 2010.

[21] W. X. Jiang, H. F. Ma, Q. Cheng, and T. J. Cui, "Illusion media: generating virtual objects using realizable metamaterials," *Applied Physics Letters*, vol. 96, no. 12, Article ID 121910, 2010.

[22] T. Yang, H. Chen, X. Luo, and H. Ma, "Superscatterer: enhancement of scattering with complementary media," *Optics Express*, vol. 16, no. 22, pp. 18545–18550, 2008.

[23] W. X. Jiang, H. F. Ma, Q. Cheng, and T. J. Cui, "Virtual conversion from metal object to dielectric object using metamaterials," *Optics Express*, vol. 18, no. 11, pp. 11276–11281, 2010.

[24] W. X. Jiang and T. J. Cui, "Radar illusion via metamaterials," *Physical Review E*, vol. 83, no. 2, Article ID 026601, 2011.

[25] W. X. Jiang, T. J. Cui, X. M. Yang, H. F. Ma, and Q. Cheng, "Shrinking an arbitrary object as one desires using metamaterials," *Applied Physics Letters*, vol. 98, no. 20, Article ID 204101, 2011.

[26] C. Li and F. Li, "Two-dimensional electromagnetic cloaks with arbitrary geometries," *Optics Express*, vol. 16, no. 17, pp. 13414–13420, 2008.